Chemistry and Physics of Lipids 214 (2018) 15–23

Contents lists available at ScienceDirect

Chemistry and Physics of Lipids

journal homepage: www.elsevier.com/locate/chemphyslip

How cardiolipin peroxidation alters the properties of the inner mitochondrial membrane?

Marjut Vähäheikkilä[a], Tapio Peltomaa[a], Tomasz Róg[a,b], Mario Vazdar[c], Sanja Pöyry[a], Ilpo Vattulainen[a,b,d,*]

[a] Laboratory of Physics, Tampere University of Technology, P.O. Box 692, FI-33101 Tampere, Finland
[b] Department of Physics, University of Helsinki, P.O. Box 64, FI-00014, Finland
[c] Division of Organic Chemistry and Biochemistry, Ruđer Bošković Institute, Bijenička 54, 10000 Zagreb, Croatia
[d] MEMPHYS – Center for Biomembrane Physics

ARTICLE INFO

Keywords:
Cardiolipin
Membrane structure
Molecular dynamics simulation
Atomistic simulation
Oxidation
Lipid bilayer

ABSTRACT

Cardiolipins have multiple vital functions within biological cell membranes, most notably in the energy metabolism associated with the inner mitochondrial membrane. Considering their essential role, peroxidation of cardiolipins may plausibly have significant effects, as peroxidation is known to alter the functionality of lipid molecules. We used atomistic molecular dynamics simulations to study how peroxidation of cardiolipin affects the properties of the inner mitochondrial membrane. To this end, we explored what happens when varying fractions of fatty acid chains of cardiolipin are replaced by its four different oxidized products in systems modeling the inner mitochondrial membrane. We found that the oxidation of cardiolipin leads to a conformational change both in the backbone/head group and in chain regions of oxidized cardiolipin molecules. The oxidized groups were observed to shift closer to the membrane–water interface region, where they formed hydrogen bonds with several other groups. Additionally, the conformational change turned out to decrease bilayer thickness, and to increase the area per lipid chain, though these changes were minor. The acyl chain conformational order of unoxidized lipids exposed to interactions with oxidized cardiolipins was increased in carbons 3–5 and decreased in carbons 13–17 due to the structural reorganization of the cardiolipin molecules. Overall, the results bring up that the conformation of cardiolipin is altered upon oxidation, suggesting that its oxidation may interfere its interactions with mitochondrial proteins and thereby affect cardiolipin-dependent cellular processes such as electron and proton transport.

1. Introduction

Cardiolipin (CL) is a fascinating lipid molecule with a unique structure consisting of two phosphatidyl groups bridged by a glycerol group. This dimeric structure includes altogether three glycerol backbones and four acyl chains (Houtkooper and Vaz, 2008; Lemmin et al., 2013). Additionally, in most mammalian tissues and higher plants, the fatty acid structure of CLs is restricted to chains including 18 carbons (Horvath and Daum, 2013), resulting in a symmetrical structure. Therefore, CL has a very special ultrastructure that is unique among phospholipids (Houtkooper and Vaz, 2008).

Cells invest eminent amount of energy to synthesize different lipids (van Meer et al., 2008), and it has been established that lipids interact specifically with membrane proteins and regulate their function (Manna et al., 2016; Lucero and Robbins, 2004; Contreras et al., 2011; Shinzawa-Itoh et al., 2007). Cardiolipin is primarily localized to membranes that have coupled electron transport and phosphorylation: bacterial plasma membranes, chloroplasts, chromatophores, and mitochondria (Hoch, 1992). CL has several vital functions especially in the energy metabolism associated with the inner mitochondrial membrane (IM) (Houtkooper and Vaz, 2008; Dahlberg and Maliniak, 2008). In energy production, CL affects, e.g., the stability of the involved enzymes and enzyme complexes (Houtkooper and Vaz, 2008). Moreover, CL is important for the stability of biological membranes (Schlame et al., 2000) and CL and its oxidation products are involved in signaling in mitochondria (Schug and Gottlieb, 2009; Tyurina et al., 2014). Considering the multitude of essential roles that CLs have in the human body, it is hardly surprising that derangements in its metabolism and composition have been associated with various pathological conditions (Claypool and Koehler, 2012), such as aging, Barth syndrome (Houtkooper et al., 2009), ischemia (Lesnefsky et al., 2009), and heart failure (Sparagna and Lesnefsky, 2009).

* Corresponding author at: Laboratory of Physics, Tampere University of Technology, P.O. Box 692, FI-33101 Tampere, Finland.
E-mail address: ilpo.vattulainen@helsinki.fi (I. Vattulainen).

https://doi.org/10.1016/j.chemphyslip.2018.04.005
Received 6 February 2018; Accepted 29 April 2018
Available online 01 May 2018

Previous studies have revealed that lipid oxidation affects the physiological functions of cell membranes and has a role in cellular membrane damage (Kulig et al., 2016; Jurkiewicz et al., 2012; Wong-ekkabut et al., 2007; Mylonas and Kouretas, 1999; Siani et al., 2016). Lipid peroxidation is thought to be linked to cellular aging and various health issues such as Parkinson's and Alzheimer's disease, schizophrenia, atherosclerosis, and inflammatory diseases (Mylonas and Kouretas, 1999; Kulig et al., 2016; Kuloglu et al., 2002). Several reactive oxygen species, such as hydroxyl radicals or hydrogen peroxides, are thought to be the main culprits (Mylonas and Kouretas, 1999). The end-products of lipid peroxidation reactions can be perilous for the viability of cells. Due to its high content of unsaturated acyl chains (Claypool and Koehler, 2012) and its location near the production site of reactive oxygen species, CL is known to be particularly susceptible to oxidation (Paradies et al., 2009). Specifically, CL oxidation is catalyzed by cytochrome c in the early stages of apoptosis, see e.g. (Kagan et al., 2005). Indeed, prevention of CL oxidation may be a promising target for new therapies (Ji et al., 2012). Further, let us stress that to the best of the authors' knowledge, no atomistic simulation studies regarding CL peroxidation in mitochondrial-like bilayer membranes have been published prior to this work. However, one study employing coarse-grained simulations recently addressed the interactions of oxidized CL with cytochrome c (Mohammadyani et al., 2018).

Previous studies suggest that oxidation of lipids alters the properties of membranes for instance by changing membrane fluidity, thickness, lipid organization, and lipid-lipid interactions (Kulig et al., 2016, 2015; Siani et al., 2016; Jurkiewicz et al., 2012). The oxidation of membrane lipids may even lead to formation of pores and membrane disruption (Runas and Malmstadt, 2015; Boonnoy et al., 2015; Caetano et al., 2007; Cwiklik and Jungwirth, 2010; Lis et al., 7563). According to simulation studies, the oxidation of membrane lipids generally increases area per lipid, decreases bilayer thickness, and it shifts oxidized groups towards the membrane–water interface of the bilayer (Siani et al., 2016; Guo et al., 2016; Wong-ekkabut et al., 2007; Garrec et al., 2014; Khandelia and Mouritsen, 2009). Nonetheless, even though oxidized lipids have been found to expose a threat for the viability of cells, the exact mechanisms of membrane damage induced by oxidation are still unclear.

This study concentrates on resolving the effects of CL oxidation on the properties of the inner mitochondrial (IM) membrane. Understanding the effects of cardiolipin peroxidation in this context is essential, since lipid peroxidation and abnormalities in cardiolipin metabolism are linked to dysfunction of biological membranes, thereby affecting human health (Lidman et al., 2016).

Given the atomistic resolution needed to explore this topic, we employ atomistic molecular dynamics (MD) simulations that can provide significant added value to complement related experimental work. Recent computational studies in membrane biophysics and physical chemistry have shown the superior capacity of atomistic computer simulations in clarifying molecular-scale mechanisms of membrane dynamics and function over time scales close to a millisecond (Manna et al., 2016; Javanainen et al., 2017). Here our approach is more modest in terms of simulation time scales, yet we consider the consequences of CL oxidation in a systematic manner by focusing on a variety of structural membrane properties that are known to be decisive for the stability of mitochondrial membranes.

We carried out atomistic MD simulations of nine different systems, eight of which included oxidized CLs and one was used as a control system based on pristine CL. The lipid content of the model systems mimicked the lipid composition of the natural inner mitochondrial membrane. To the best of the authors' knowledge, no simulation studies regarding cardiolipin peroxidation in mitochondrial-like bilayer membranes have been published prior to this work.

We found that the oxidation of one of the acyl chains of CL alters the structural properties of the inner mitochondrial-like membranes. Key membrane properties such as membrane thickness, membrane area, and lipid conformational order were found to be modulated by CL oxidation, however the effects were minor, and perhaps even surprisingly minor. It therefore turned out that the effects of CL oxidation are not exceptionally profound in the overall membrane properties, yet oxidation of CL was observed to give rise to a significant effect, which likely has a role in interfering with biological functions: we found CL oxidation to change the conformation of CL by altering its orientation in a membrane. Given that CL is known to bind various mitochondrial proteins and thereby contribute to their function, it is quite plausible that the observed oxidation-induced change in CL conformation may alter CL–protein interactions and hence affect biological processes where CL plays a role, such as proton and electron transport.

2. Methods

2.1. Bilayer setup and simulations

To characterize the effect of cardiolipin oxidation on the structure and properties of the IM membrane, we considered nine different model systems. The models were based on the natural composition of the IM membrane, which includes phosphocholines, phosphoethanolamines, and cardiolipins as main lipid components (Hallermayer and Neupert, 1974; Daum, 1985). Thus, all bilayers in our models contained 47.4 mol % 1,2-di-(9Z,12Z-octadecadienoyl)-*sn*-glycero-3-phosphocholine (DLPC), 40.4 mol% 1,2-di-(9Z,12Z-octadecadienoyl)-*sn*-glycero-3-phosphoethanolamine (DLPE), and 12.3 mol% cardiolipin molecules, whose structures are presented in Fig. 1. The models mimic the natural composition of the inner mitochondrial membrane (Daum, 1985). The molar concentrations given above result in 54 DLPC, 46 DLPE, and 14 CL molecules, totaling to 114 lipids in a bilayer. The acyl chains of all lipids were unsaturated and included 18 carbons with double bonds at positions 9 and 12 (linoleic acid, 18:2c9,12). The total charge of CL in physiological conditions is controversial (Dahlberg et al., 2010; Kates et al., 1993; Olofsson and Sparr, 2013), and both single and double charged CLs have been proposed. In our model, CL carried a charge of −2e. The model was introduced and verified elsewhere (Róg et al., 2009) and later used in the study of Pöyry et al. (Pöyry et al., 2009).

In the simulation models, we substituted one chain of 6 or 14 cardiolipins with one of four different oxidized products of linoleic acid, thus obtaining eight systems including oxidized cardiolipins, see Table 1. The used oxidized products were hydroperoxide and aldehyde groups (see Fig. 2): 13-hydroperoxy-*trans*-11,*cis*-9-octadecadienoic acid (13-tc); 9-hydroperoxy-*trans*-10,*cis*-12-octadecadienoic acid (9-tc); 12-oxo-*cis*-9-dodecenoic acid (12-al); and 9-oxo-nonanoic acid (9-al). Usually the polyunsaturated chains, and thus their oxidized products, are connected to the *sn*-2 carbon in lipids. In this study, we placed the oxidized products in the *sn*-1 position, as it has been observed to be more prone to oxidation in CL-containing four linoleoyl tails (Maciel et al., 2011). The control system did not include any oxidized lipids.

Altogether, we obtained a total of 9 different systems where the concentration of oxidized CL was 0 ('Control' in Table 1), 5.3 mol% ('Low'), or 12.3 mol% ('High'), as listed in Table 1. The given CL concentrations were chosen so as to sample the extremes of the concentration range.

For lipids and ions, we used the all-atom OPLS (Optimized Parameters for Liquid Simulations) force field (Kaminski et al., 2001) using additional parameters specifically derived for lipids (Maciejewski et al., 2014; Kulig et al., 2016, 2015; Róg et al., 2016). For water, we used the TIP3P model (Jorgensen et al., 1983).

For the oxidized products of linoleic acid, additional parameters were needed, see the highlighted fragment in Fig. 2. Partial atomic charges were derived in accordance with the OPLS methodology by fitting to the electrostatic potential using the RESP procedure (Dupradeau et al., 2010), and torsion angle parameters were derived using the procedure described by Maciejewski et al. (Maciejewski et al., 2014). All electronic calculations were performed with second order

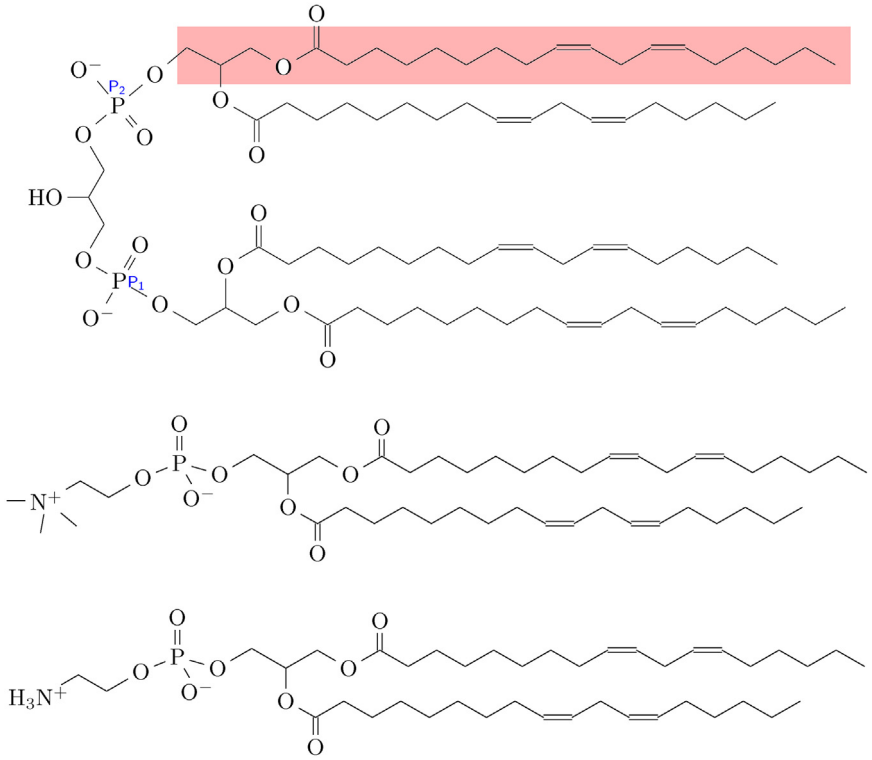

Fig. 1. The structure of (top) cardiolipin, (middle) DLPC, and (bottom) DLPE molecules considered in this work. The red area indicates the chain that is modified in oxidized systems. (For interpretation of the references to color in this figure legend, the reader is referred to the web version of the article.)

Table 1
Abbreviations used for the systems, including their CL content.

System name	Number of CL molecules	Oxidized product of linoleic acid in an oxidized CL chain
13-tc$_{High}$	14 oxidized CLs	13-tc
13-tc$_{Low}$	8 pristine CLs + 6 oxidized CLs	13-tc
9-tc$_{High}$	14 oxidized CLs	9-tc
9-tc$_{Low}$	8 pristine CLs + 6 oxidized CLs	9-tc
12-al$_{High}$	14 oxidized CLs	12-al
12-al$_{Low}$	8 pristine CLs + 6 oxidized CLs	12-al
9-al$_{High}$	14 oxidized CLs	9-al
9-al$_{Low}$	8 pristine CLs + 6 oxidized CLs	9-al
Control	14 pristine CLs	–

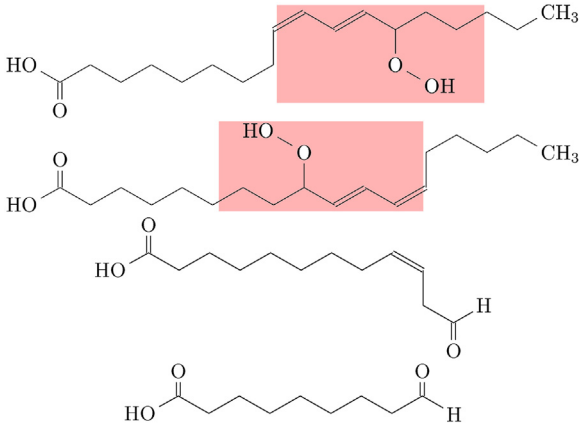

Fig. 2. The products of the oxidation of linoleic acid taken into account in this study. From top to bottom: 13-hydroperoxy-*trans*-11,*cis*-9-octadecadienoic acid (13-tc), 9-hydroperoxy-*trans*-10,*cis*-12-octadecadienoic acid (9-tc), 12-oxo-*cis*-9-dodecenoic acid (12-al), and 9-oxo-nonanoic acid (9-al). The red areas indicate the fragment for which additional simulation parameters were derived by quantum-mechanical calculations (see text). (For interpretation of the references to color in this figure legend, the reader is referred to the web version of the article.)

Møller-Plessent perturbation theory (MP2) with the 6-31G** basis set within the Gaussian 03 program (Frisch et al., 2004). In more practical terms, the electronic calculations were performed using the procedure described in Maciejewski et al. (2014), the energies in question being given schematically by [E(CCSD(T)/LBS) = E(CCSD(T)/SBS) + (E(MP2/LBS) − E(MP2/SBS))], where LBS is an abbreviation for the cc-pVTZ basis set and SBS is an abbreviation for the cc-pVDZ basis set. Final CCSD(T)/LBS energies were used in the fitting procedure. The derived parameters are given in the Supporting Information (SI) as a part of molecular topologies.

When building the systems, we arranged the lipids in an array in the bilayer *xy*-plane, so that both leaflets contained the same number of each lipid species. We hydrated all bilayers with 3586 water molecules and added 28 sodium ions (Na^+) to neutralize the total charge of the systems. Altogether, the systems comprised between 26796-27160 atoms.

Prior to MD simulations, we minimized the energies of the initial structures by using the steepest descent algorithm. Three repetitions of each simulation with different initial velocities were performed to confirm reproducibility. The integration time step was 2 fs. The simulations were performed at a constant semi-isotropic pressure (1 bar) with a compressibility of 4.5×10^{-5} and at a constant temperature (310 K). The pressure was controlled using the Parrinello–Rahman (Parrinello and Rahman, 1981) barostat and temperature with the Nosé–Hoover (Nosé, 1984) thermostat with time constants 1.0 ps and 0.4 ps, respectively.

Periodic boundary conditions were applied in all three dimensions.

A cutoff of 1.0 nm was applied to Lennard–Jones interactions. Electrostatic interactions were treated using the Particle-Mesh Ewald method. The neighbor list was updated every 10th step and the LINCS (Hess et al., 1997) algorithm was used to constrain the bond lengths.

All simulations were performed over a period of 600 ns with the GROMACS software package (Berendsen et al., 1995) (version 4.6.5). We monitored equilibration by considering the time development of the area per lipid that settled to equilibrium values in less than 300 ns in all simulations. Thus, the first 300 ns of each simulation was considered as the equilibration period and the last 300 ns was analyzed. The total simulation time of the full project was about 16 µs.

2.2. Analysis methods

Analysis was conducted using the GROMACS software package (Berendsen et al., 1995), VMD (Humphrey et al., 1996), and the authors' own software.

In MD studies, the area per lipid (in the *xy*-plane) is typically given as total area divided by the number of lipids in one leaflet. Here, we instead calculated the area per lipid chain, since there are four hydrocarbon chains in CL and only two in DLPE and DLPC lipids. Area per chain is calculated by dividing the total area of the bilayer by the number of lipid chains in a single leaflet.

Moreover, we calculated a related quantity, the thickness of the membrane (along the *z*-direction), using electron density profiles that were computed across the membrane separately for water molecules and all lipids. Membrane thickness is then defined as the distance between the two points where the density of water equals the density of all lipids.

Additionally, to explore how individual structural units in the lipid molecules were distributed inside a membrane, along its normal direction, we examined the electron density profiles of several individual components. The results were averaged over the two leaflets of each membrane (all membranes were symmetric) and scaled so that the maximum value equals one to make comparison easier.

Hydrogen bonds were defined geometrically: a hydrogen bond is here considered to exist when the donor and the acceptor are at most 0.325 nm apart and the bond angle is at most 30 degrees.

To characterize the order of lipid acyl chains, we calculated the deuterium order parameter (S_{CD}):

$$S_{CD} = \frac{3}{2}\left\langle \cos^2\theta - 1 \right\rangle, \tag{1}$$

where θ is the angle between a CH-vector and the bilayer normal. The brackets indicate that order parameter is averaged over all studied lipids and time. Order parameters are calculated separately for the unoxidized *sn*-1 chains of oxidized lipids and for *sn*-1 chains of unoxidized lipids.

To study the conformation of oxidized CLs, we calculated angles between the outward bilayer normal and a vector between the CL phosphorus atoms (Fig. 1). We also calculated the angle between the PN-vector of DLPC and DLPE molecules (Fig. 1) and the outward bilayer normal to analyze the head group orientation of these lipids.

Radial distribution functions (RDFs) and coordination numbers were calculated to analyze the possible reorganization of membranes including oxidized CLs compared with the control system. All RDFs were computed in three dimensions. The coordination number gives the number of atoms of a given species in the first shell around the studied group by evaluating the integral

$$N = \int_0^{r_{\min}} \mathrm{d}r\, 4\pi\rho g(r) r^2, \tag{2}$$

where r is the radial distance, ρ is the average number density of studied atoms, $g(r)$ is the RDF. The quantity $r_{\min}$ denoting the radius of the first shell is taken as the distance of the first minimum of the RDF of the studied atoms around a specific group.

We computed the charge density across the system by dividing the system into slices in the direction of the bilayer normal (z) and counting the number of charges in each slice. Further, we obtained the electrostatic potential by integrating the charge profile twice from the water phase toward bilayer center to attain the electrostatic potential (Gurtoveko and Vattulainen, 2009)

$$\Phi(z) - \Phi(0) = \frac{-1}{\varepsilon_0}\int_0^z \int_0^{z'} \mathrm{d}z''\mathrm{d}z'\rho(z''), \tag{3}$$

where ε_0 is the vacuum permittivity and ρ is the charge density.

We averaged all results over the three simulation repetitions that were carried out for each system. Errors for the area per chain, membrane thickness, and hydrogen bonds were calculated separately for each repetition with the block averaging method described by Hess (2002). The presented error is the largest error obtained from the three repetitions.

3. Results and discussion

3.1. Cardiolipin peroxidation causes conformational changes to lipid chains

We found that the most notable change in the simulations including oxidized CLs is that the conformation of the oxidized CL chains changes: the oxidized groups within the chains shift toward the membrane–water interface from the more inner parts of the bilayer. Two examples of final structures where this conformational change is evident are

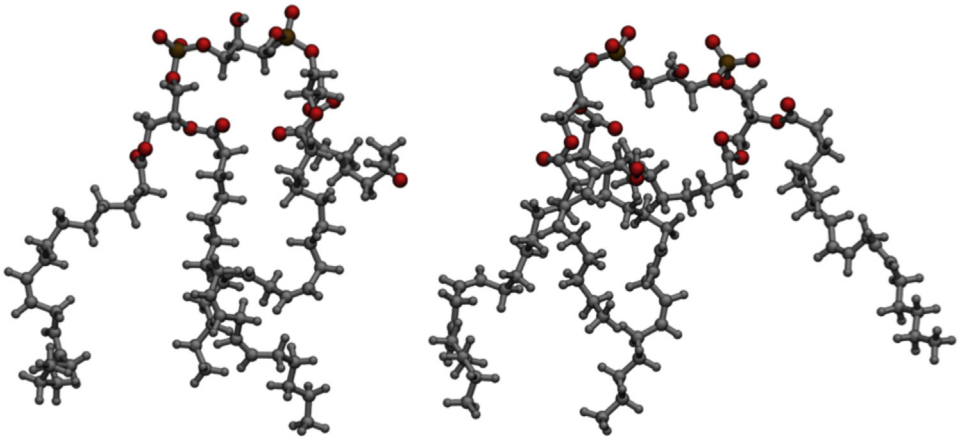

Fig. 3. Snapshots of simulations demonstrating typical final conformations of oxidized cardiolipin molecules in (left) 9-al$_{High}$ and (right) 9-tc$_{High}$ systems. Carbon atoms are shown in silver, oxygen atoms in red, and phosphate atoms in ochre. The figure was created using VMD (Humphrey et al., 1996).

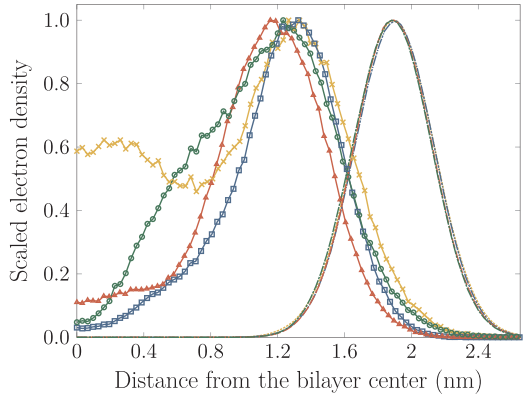

Fig. 4. The electron density profiles for oxygen atoms in 13-tc_{High} peroxide group (red triangle), 9-tc_{High} peroxide group (blue square), 12-al_{High} aldehyde group (yellow cross), 9-al_{High} aldehyde group (green circle), and phosphate oxygens of lipids in 13-tc_{High} (red – –), 9-tc_{High} (blue – · –), 12-al_{High} (yellow · · · ·), and 9-al_{High} (green – · –) system. (For interpretation of the references to color in this figure legend, the reader is referred to the web version of the article.)

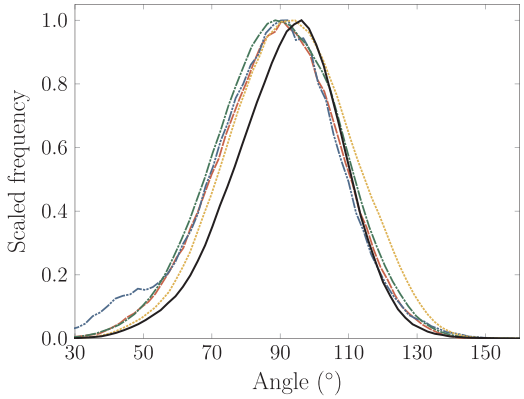

Fig. 5. The distribution of angles between the bilayer outward normal and the vector between the phosphorus atoms of CL in 13-tc_{High} (red – –), 9-tc_{High} (blue – · –), 12-al_{High} (yellow · · · ·), 9-al_{High} (green – · –), and control systems (black ——). (For interpretation of the references to color in this figure legend, the reader is referred to the web version of the article.)

shown in Fig. 3. As the oxidized group twists outward, the orientation of the whole lipid chain changes. As described later, this affects the conformation of the entire CL molecule. As unoxidized chains do not undergo this conformational change, the oxidized lipid chains are located, on average, closer to the membrane–water interface compared to other lipid chains.

We verified the twist of oxidized groups toward the head group region by examining the electron density profiles of aldehyde and peroxide groups in the different systems, as shown in Fig. 4. For clarity, it depicts the results for systems that included the largest number of oxidized CLs (12.3 mol%), but a similar pattern is also seen in systems including a smaller amount of oxidized CLs (5.3 mol%). Additionally, the electron density profile of phosphate oxygens is shown in the same figure to clarify the overall structure.

The oxidized group is at the end of the chain in aldehyde-containing systems but at different positions along the chain in the peroxide systems, see Fig. 4. Despite this, there are no significant differences in the profiles of phosphate oxygens in the distinct oxidized systems. However, the distributions of different oxidized groups vary from one system to another. Even though the oxidized groups are at the end of the chains in aldehyde-containing systems, the highest density of these groups is nearer the highest density of phosphate oxygens than the bilayer center. The distributions of aldehyde groups (-al) are wider compared to peroxide groups (-tc). The oxidized groups shift closer to the membrane–water but are, on average, located deeper inside the membrane than phosphate oxygens in all systems.

Previously, the conformational change of oxidized lipid chains were studied for 1-palmitoyl-2-lineoleoyl-*sn*-glycero-3-phosphatidylcholine (PLPC) lipids (Wong-ekkabut et al., 2007), which were oxidized with similar oxidation products of linoleic acid as in this study. Additionally, Garrec et al. (2014) and Jarerattanachat et al. (2013) performed MD simulations of DLPC and PLPC bilayers containing oxidized lipids, respectively. All of these studies reported the bending of oxidized chains toward the membrane–water interface. The oxidized groups were found, on average, near the interface region but deeper inside the membrane than the phosphate groups (Wong-ekkabut et al., 2007; Garrec et al., 2014), in agreement with our results. Similarly to our results, Wong-ekkabut et al. (2007) and Boonnoy et al. (2015) found that the distribution of oxidized groups is wider for aldehyde-containing lipids than peroxide-containing lipids. On average, the peroxide groups prefer to stay closer to the membrane–water interface compared to the aldehyde groups. Plausible reasons for the differences in the distributions include the physical size of the chains and the different solubility properties of aldehyde and peroxide groups. Peroxide groups are more hydrophilic than aldehyde groups. Furthermore, the aldehyde groups are located at the end of the chains, and the lengths of the chains containing them are shorter than those of peroxide oxidized chains.

3.2. Oxidation of one fatty acid chain in cardiolipin induces a conformational change in the whole cardiolipin molecule

We calculated the angle between the outward bilayer normal and a vector between the phosphorus atoms P_1 and P_2 ($\overrightarrow{P_1P_2}$, see Fig. 1) in CL to study how the conformation of CL changes due to their oxidation, see Fig. 5. The distribution of angles between the vector from cardiolipin phosphorus atom to another and the bilayer outward normal is wider for the oxidized systems than in the control system. Therefore, the orientation of the oxidized cardiolipins is asymmetric more often than in the case of unoxidized CLs. On average, P_2 atoms are located closer to the interface region than P_1 atoms. However, as seen from the widened distributions, oxidation of CL can induce tilting in both directions (there are tilt angles both below and above 90°).

We also calculated the electron density profiles separately for both of the cardiolipin phosphorus atoms. The data shown in SI indicate that in the control system the electron density profiles of the two phosphorus atoms are nearly identical, indicating a nearly symmetric orientation of CL molecules. In contrast, in the oxidized systems some of the profiles of the phosphorus atoms are widened and/or shifted compared to the corresponding profiles in the control system. In all of the oxidized systems, either one or both phosphorus profiles are wider as compared to the corresponding profile in the control system, indicating a less well-defined location of the phosphorus atoms. These results are in agreement with the angle distributions (Fig. 5) and indicate oxidation-induced changes in the orientation of cardiolipins.

According to the results of the electron density profiles and angle distribution analyses, the oxidation of CLs induces tilting of the whole CL molecule. Several features of CL imply that some functional roles of CL may be affected by these changes.

First of all, the restriction of the eukaryotic fatty acid pattern of CL, so that all chains are symmetric in length (Schlame et al., 2000), suggests that some degree of symmetry in the CL conformation may be required for proper function. CL has been suggested to have a role as a proton trap and conductor within mitochondrial membranes (Haines and Dencher, 2002), and indeed, the effect of CL conformation on the proton binding properties has been studied by Dahlberg and Maliniak (2010). Additionally, cardiolipins have important interactions with proteins, for example with respiratory complexes (Schwall et al., 2012) and cytochrome c (Hanske et al., 2012). Plausibly, changes in CL conformation due to oxidation might alter its interactions with other

Table 2
Results for the average area per chain and bilayer thickness. Error bars have been evaluated using the block averaging method (Hess, 2002).

System name	Average area per chain (nm^2)	Average thickness (nm)
13-tc_{High}	0.318 ± 0.005	4.05 ± 0.02
13-tc_{Low}	0.315 ± 0.004	4.09 ± 0.03
9-tc_{High}	0.318 ± 0.004	4.05 ± 0.03
9-tc_{Low}	0.315 ± 0.004	4.10 ± 0.07
12-al_{High}	0.314 ± 0.002	4.04 ± 0.04
12-al_{Low}	0.312 ± 0.001	4.10 ± 0.06
9-al_{High}	0.311 ± 0.003	4.05 ± 0.05
9-al_{Low}	0.312 ± 0.002	4.09 ± 0.02
Control	0.312 ± 0.002	4.11 ± 0.02

molecules, including proteins.

The oxidation of CL may also affect the conformation of other lipids in the same membrane. We examined the effects on DLPC and DLPE head group orientations by computing their head group tilt angles. The angles were computed between the PN-vectors of the lipids and the outward bilayer normal for both lipid types. We found that the angle distributions are not significantly influenced by the addition of oxidized CLs, at least for the low concentrations of the oxidized lipids studied here.

3.3. Oxidation of CL decreases the bilayer thickness

We examined the average area per chain and bilayer thickness, see Table 2. The bilayer thickness is decreased in every system containing 14 oxidized CLs (12.3 mol%) when compared with the control system. In systems including 6 oxidized CLs (5.3 mol%), one can observe the same trend, though for this lower CL concentration the effect weaker, as expected.

The differences in the area per chain values are modest between the different systems (see Table 2). The average area per chain values are higher for most of the oxidized systems compared with the control system, however the differences fall largely within the error bars. Plausibly, the differences in the bilayer thickness and area per chain results are at least partly due to the different lengths of the oxidized lipid chain. Aldehyde-containing CLs include a shorter oxidized chain than CLs that contain a peroxide group, which may explain why the area per chain is slightly smaller in systems containing the aldehyde group. Nonetheless, altogether one can find that oxidation of CL leads to increasing area that is compensated by decreasing membrane thickness, such that the membrane volume remains largely constant. These effects are the stronger the more oxidized CL there is in a membrane.

Similarly to our results, the decrease in bilayer thickness upon addition of oxidized lipids has been observed in other MD studies (Wong-ekkabut et al., 2007; van der Paal et al., 2016; Khandelia and Mouritsen, 2009; Guo et al., 2016). Wong-ekkabut et al. (2007) showed that membrane thickness decreases as the concentration of oxidized PLPC increases. van der Paal et al. (2016) and Khandelia and Mouritsen (2009) observed a similar phenomenon for oxidized POPC lipids. Guo et al. (2016) found that complete peroxidation of pure POPC and DOPC bilayers leads to decrease in bilayer thickness.

Multiple other MD studies have shown that oxidation of membrane lipids may affect area per lipid values (Wong-ekkabut et al., 2007; van der Paal et al., 2016; Khandelia and Mouritsen, 2009). The area per lipid results seem to depend on the studied oxidation products. In the studies of van der Paal et al. (2016), and Khandelia and Mouritsen (2009), the area per lipid is increased or decreased as a function of oxidized lipid concentration depending on the oxidation product and the concentration of oxidized lipids. Wong-ekkabut et al. (2007) found that the area per lipid increased as the concentration of studied oxidation products increased. Guo et al. (2016) showed that complete peroxidation of pure POPC and DOPC bilayers increases area per lipid values.

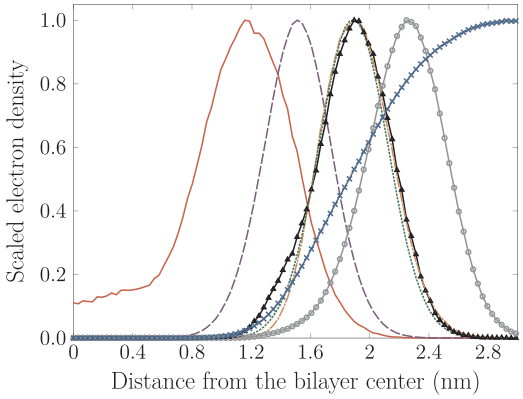

Fig. 6. The electron density profile of oxygen atoms in aldehyde group (red ——), oxygen atoms in ester (purple – –), CL head group (black triangle), amine (brown –·–), oxygen atoms in phosphate group (green · · · ·), choline (gray circle), and water (blue cross) in the 13-tc_{High} system containing 12.3 mol% of oxidized CL. (For interpretation of the references to color in this figure legend, the reader is referred to the web version of the article.)

3.4. Cardiolipin head groups are located as deep as amine and phosphate groups in the bilayers

We calculated the electron density profiles for the oxygens of oxidized groups, ester oxygens, phosphate oxygens, choline, amine, water, and CL head group. As a representative example, the profiles are illustrated for the 13-tc_{High} in Fig. 6. According to the density profiles, the CL head groups are located as deep as phosphate and amine groups in the membranes. The outermost group after water is choline, and ester oxygens are located, on average, between CL oxidized groups and CL head groups.

The differences in the density profiles between different systems are very small including the control system, except for the oxidized groups shown in Fig. 4. Therefore, the relative locations of lipid functional groups are unaffected by oxidation of CL chains. Especially of interest, the relative location of the CL head group is the same irrespective of oxidation. According to the density profiles, water seems to penetrate slightly deeper into the membrane when the system includes oxidized CLs compared with the control system. To check as to whether this is simply due to the thinning of the membrane, or if the water molecules actually penetrate deeper into the bilayer, we further analyzed the location of water molecules. We calculated the RDFs separately for water molecules around the following groups: ester, phosphate, choline, and amine. There were no significant differences in these distributions between the control system and the oxidized systems. We also studied whether water penetrates deeper into membrane close to oxidized groups than farther away of them but the differences were not significant. Consequently, the small differences in the water density profiles seem to be due to the different thicknesses of the membranes, and water permeation is not observed.

Lis et al., 2011Lis et al. (7563) showed that significant water permeation takes seconds when oxidation ratio is 15 mol%. Further, when the oxidation ratio is 75 mol%, spontaneous pore formation was observed at the time scale of tens of nanoseconds (Lis et al., 7563). In our simulations, at the most 12.3 mol% of lipids were oxidized. Moreover, the simulation time is 600 ns which may not be long enough to observe pore formation or significant water permeation with an oxidation ratio of 12.3 mol% or less.

Electron density profiles were calculated also for sodium ions in all systems. Sodium ions are located, on average, deeper in the bilayer than amine groups but closer to the membrane–water interface than ester

groups. To study the possible differences in the spatial location of the sodium ions, we calculated the RDFs separately for sodium ions around the following groups: water, ester, phosphate, and cardiolipin head group. The only significant differences occurred in the RDF profiles for sodium atoms around cardiolipin head groups, however the results were inconclusive and we were not able to find a clear pattern. Moreover, we remain skeptical of whether the time scale in our simulations is sufficient to probe this phenomenon.

To see whether the oxidation of CL chains has any effect on the relative locations of the head groups of different lipid species, we calculated the electron density profiles of DLPE and DLPC phosphorus atoms. The phosphorus atoms of both DLPE and DLPC shift approximately 0.05 nm closer to the bilayer center in systems including 14 oxidized CLs (12.3 mol%) compared with the control system. This difference corresponds approximately to the changes in the thickness of the membrane (see Table 2).

3.5. CL oxidized groups form hydrogen bonds especially with water

The conformational change of the oxidized chains towards the water phase enables the aldehyde groups to form hydrogen bonds with water. Similarly, peroxide groups then favor hydrogen bonds especially with water, carbonyl groups, and phosphate groups. Additionally, a few hydrogen bonds were observed between the oxidized groups and DLPE amine groups and cardiolipin head groups, but these hydrogen bonds were only incidental and, thus, the data are not presented here. Table 3 shows the average hydrogen bonds per oxidized group. All oxidized groups form hydrogen bonds most considerably with water. Peroxide groups form more hydrogen bonds with ester groups than phosphate groups. The differences in the number of hydrogen bonds in systems containing 5.5 and 12.3 mol% of oxidized CL are small and fall within the error bars in most of the systems. However, peroxide groups form considerably more hydrogen bonds with water than the aldehyde groups do. This is probably due to the location of the oxidized groups: peroxide groups are on average located closer to the membrane–water interface than aldehyde groups, see Fig. 4.

Similarly to our results, Wong-ekkabut et al. (2007) found in their study on PLPC oxidation that oxidized groups form the most hydrogen bonds with water, and additionally with carbonyl and phosphate groups. In their study, peroxide groups generally formed more hydrogen bonds with phosphate groups than with ester groups. This difference may be due to the greater shift of PLPC oxidized chains toward the membrane–water interface than CL oxidized groups in our study and therefore the PLPC oxidized groups are on average located closer to the phosphate groups than oxidized groups of CLs in this work. Consequently, when oxidized groups are located deep inside the membrane, more hydrogen bonds are observed between oxidized and ester groups than with phosphate groups, since ester groups are located deeper in the bilayer than phosphate groups.

Table 3
Average number of hydrogen bonds between hydroperoxide or aldehyde groups and the specified group per oxidized lipid chain in each system. Error estimates were evaluated using the block averaging method.

System name	Water	Ester group	Phosphate group
13-tc_{High}	0.62 ± 0.04	0.38 ± 0.10	0.03 ± 0.04
13-tc_{Low}	0.6 ± 0.3	0.34 ± 0.04	0.03 ± 0.02
9-tc_{High}	0.77 ± 0.05	0.26 ± 0.04	0.08 ± 0.05
9-tc_{Low}	0.9 ± 0.2	0.22 ± 0.03	0.11 ± 0.05
12-al_{High}	0.16 ± 0.01	–	–
12-al_{Low}	0.18 ± 0.02	–	–
9-al_{High}	0.16 ± 0.02	–	–
9-al_{Low}	0.21 ± 0.02	–	–

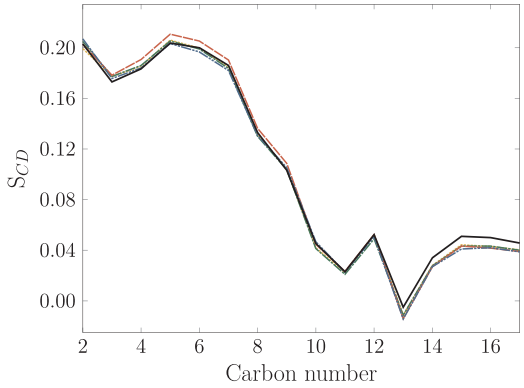

Fig. 7. Order parameters of unoxidized lipids' *sn*-1 tail in 13-tc_{High} (red – –), 9-tc_{High} (blue – · –), 12-al_{High} (yellow · · · ·), 9-al_{High} (green – – –), and in the control system (black ——). Error bars are smaller than the line thickness. (For interpretation of the references to color in this figure legend, the reader is referred to the web version of the article.)

3.6. The order of the terminal ends of cardiolipin chains decreases in membranes containing oxidized lipids

To examine the order of the bilayers, we calculated the deuterium order parameter for the *sn*-1 chains of lipids. The order parameter was calculated separately for oxidized lipids' unoxidized *sn*-1 chains and for the *sn*-1 chains of unoxidized lipids. The order parameter of the *sn*-1 chain of unoxidized lipids is shown in Fig. 7 for the control system. Every system including 5.3 or 12.3 mol% of oxidized lipids showed a similar pattern. The order parameter of unoxidized lipids' chains is decreased for carbons 13–17 in systems containing oxidized lipids, as compared with the control system. The differences in the lipid order parameters may be caused by the conformational change of the oxidized CL chains: as the oxidized chains turn closer to the membrane–water interface, the amount of free space is increased in the center of the bilayer and carbon atoms 13–17 in the unoxidized chains become more mobile compared with the control system.

The order of oxidized lipids' unoxidized chains is increased for carbons 3–5 in systems including oxidized lipids compared with the control system. This is reasonable since interactions are increased (see Table 3) and free space is decreased in the interface region due to the reorientation of oxidized chains.

Wong-ekkabut et al. (2007), van der Paal et al. (2016), and Khandelia and Mouritsen (2009) conclude in their MD studies regarding phospholipid oxidation that, in general, lipid order parameter decreases upon increasing oxidation of lipid molecules.

3.7. Oxidation induces only modest changes in the electrostatic potential

Electrostatic potential plays a role, e.g., in the interplay between the membrane surface and charged substances. The electrostatic potential of all system components was calculated across the bilayer as an average of the two leaflets, see Fig. 8. The differences in the potential induced by oxidation are very modest between the systems. The largest changes occur in the region, where the density of oxidized groups is the highest (0.8–1.6 nm from the bilayer center). The aldehyde-containing systems deviate more from the control system than the peroxide-containing systems. The location of charged ions and the orientation of the polar lipids affect the potential. Therefore, the effect of reorientation of polar head groups may be compensated by redistribution of ions and vice versa.

4. Conclusions

In this study, we used atomistic MD simulations to examine how CL oxidation described in terms of aldehyde or peroxide groups bound to

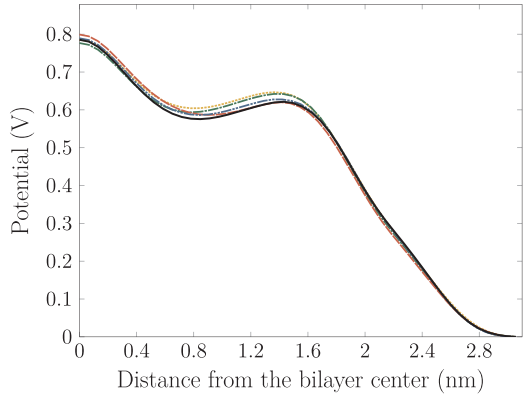

Fig. 8. Potential of all system components in 13-tc_{High} (red – –), 9-tc_{High} (blue –·–), 12-al_{High} (yellow · · ·), 9-al_{High} (green –· –), and in the control system (black ——) calculated from the water phase toward the bilayer center. (For interpretation of the references to color in this figure legend, the reader is referred to the web version of the article.)

one of CL acyl chains affects the structural properties of the inner mitochondrial membrane.

The oxidation of CL was found to cause conformational changes to the oxidized lipid chains compared to their nonoxidized counterparts. The oxidized chains underwent a major conformational change, where the chains shifted closer to the membrane–water interface region. A similar shift of oxidized lipid chains has been observed previously (Wong-ekkabut et al., 2007; Garrec et al., 2014; Jarerattanachat et al., 2013; Boonnoy et al., 2015; Guo et al., 2016) for other phospholipids. Additionally, the oxidized groups formed hydrogen bonds mainly with water. These phenomena were more pronounced for hydroperoxide lipids compared to aldehyde lipids, which likely stems from the higher hydrophilicity of the hydroperoxide group.

Interestingly, the oxidation of just one cardiolipin chain was found to induce tilting of the whole CL molecule. Eukaryotic cardiolipins have a unique fatty acid pattern that is essentially restricted to chains including 18 carbon atoms (Schlame et al., 2000), which results in symmetric chain lengths within the CL molecule. Oxidation of CL may change the chain length and induce tilting of the whole molecule, altering the symmetry of the molecule. Plausibly, this may affect the functional properties of cardiolipin, such as its suggested role as a proton trap (Haines and Dencher, 2002) in mitochondrial membranes.

The oxidation of CL also affected other structural properties of lipid bilayers. The thickness of the bilayer was decreased regardless of the length of the oxidized lipid chain, and the membrane area was slightly increased due to oxidation. Similarly to our results, membrane thinning due to oxidation of lipids has been observed in other MD studies (Wong-ekkabut et al., 2007; van der Paal et al., 2016; Khandelia and Mouritsen, 2009; Guo et al., 2016), and previous simulations have also indicated that the effect of lipid oxidation on area per lipid values depends on the studied oxidation products (van der Paal et al., 2016; Khandelia and Mouritsen, 2009).

The conformational change of oxidized CL chains increased the amount of free space in the middle of the bilayer and decreased it in the head group region. This affected the order of lipid chains. The order parameter of unoxidized lipid chains was increased for carbons 3–5 and decreased for carbons 13–17 compared with the corresponding order parameters in the control system. In general, lipid order parameter has been found to decrease upon an increasing number of oxidized lipid molecules (Wong-ekkabut et al., 2007; van der Paal et al., 2016; Khandelia and Mouritsen, 2009).

Most of the observed differences in the properties of membranes including oxidized lipids compared with the control membrane were found to be small. This is reasonable given that only 2.3 or 5.5 mol% of CL acyl chains were oxidized in the studied membrane systems. Notwithstanding of that, noteworthy differences induced by oxidation were yet observed in the present work. Of greatest interest is the observation that oxidation of CL changes its overall conformation. This may have significant consequences given that the binding of CL to various mitochondrial proteins (and in particular to protein complexes associated with the respiratory chain) is strong and likely specific (Paradies et al., 2014). Now, if the conformation of CL were altered due to oxidation, it is quite possible that the structure of oxidized CL would no longer match the structural profile of its binding pocket in the host protein, implying that the biological function, such as proton and electron transport would be impaired to a certain degree. Considering the key role of CL in several aspects of the inner mitochondrial membrane function, this calls for additional research.

Acknowledgements

We wish to thank the Academy of Finland (Center of Excellence project (Grant No. 307415)) and the European Research Council (Advanced Grant project (Grant No. 290974)) for funding, and CSC – IT Center for Science (Espoo, Finland) for ample computing resources.

Appendix A. Supplementary data

Supplementary data associated with this article can be found, in the online version, at https://doi.org/10.1016/j.chemphyslip.2018.04.005.

References

Berendsen, H.J., van der Spoel, D., van Drunen, R., 1995. GROMACS: a message-passing parallel molecular dynamics implementation. Comput. Phys. Commun. 91, 43–56.
Boonnoy, P., Jarerattanachat, V., Karttunen, M., Wong-ekkabut, J., 2015. Bilayer deformation, pores, and micellation induced by oxidized lipids. J. Phys. Chem. Lett. 6, 4884–4888.
Caetano, W., Haddad, P., Itri, R., Severino, D., Vieira, V., Baptista, M., Schröder, A., Marques, C., 2007. Photo-induced destruction of giant vesicles in methylene blue solutions. Langmuir 23, 1307–1314.
Claypool, S., Koehler, C., 2012. The complexity of cardiolipin in health and disease. Trends Biochem. Sci. 37, 32–41.
Contreras, F.X., Ernst, A.M., Wieland, F., Brugger, B., 2011. Specificity of intramembrane protein–lipid interactions. Cold Spring Harb. Perspect. Biol. 3, a004705.
Cwiklik, L., Jungwirth, P., 2010. Massive oxidation of phospholipid membranes leads to pore creation and bilayer disintegration. Chem. Phys. Lett. 486, 99–103.
Dahlberg, M., Maliniak, A., 2008. Molecular dynamics simulations of cardiolipin bilayers. J. Phys. Chem. B 112, 11655–11663.
Dahlberg, M., Maliniak, A., 2010. Mechanical properties of coarse-grained bilayers formed by cardiolipin and zwitterionic lipids. J. Chem. Theory Comput. 6, 1638–1649.
Dahlberg, M., Marini, A., Mennucci, B., Maliniak, A., 2010. Quantum chemical modeling of the cardiolipin headgroup. J. Phys. Chem. A 114, 4375–4387.
Daum, G., 1985. Lipids of mitochondria. Biochim. Biophys. Acta 822, 1–42.
Dupradeau, F.-Y., Pigache, A., Zaffran, T., Savineau, C., Lelong, R., Grivel, N., Lelong, D., Rosanski, W., Cieplak, P., 2010. The R.E.D. tools: advances in RESP and ESP charge derivation and force field library building. Phys. Chem. Chem. Phys. 12, 7821–7839.
Frisch, M.J., Trucks, G.W., Schlegel, H.B., Scuseria, G.E., Robb, M.A., Cheeseman, J.R., Montgomery Jr., J.A., Vreven, T., Kudin, K.N., Burant, J.C., et al., 2004. Gaussian 03, Revision C. 02. Gaussian, Inc, Wallingford, CT.
Garrec, J., Monari, A., Assfeld, X., Mir, L., Tarek, M., 2014. Lipid peroxidation in membranes: the peroxyl radical does not “float”. J. Phys. Chem. Lett. 5, 1653–1658.
Guo, Y., Baulin, V., Thalmann, F., 2016. Peroxidised phospholipid bilayers: insight from coarse-grained molecular dynamics simulations. Soft Matter 12, 263–271.
Gurtoveko, A.A., Vattulainen, I., 2009. Calculation of the electrostatic potential of lipid bilayers from molecular dynamics simulations: methodological issues. J. Chem. Phys. 130, 215107.
Haines, T., Dencher, N., 2002. Cardiolipin: a proton trap for oxidative phosphorylation. FEBS Lett. 528, 35–39.
Hallermayer, G., Neupert, W., 1974. Lipid composition of mitochondrial outer and inner membranes of Neurospora crassa. Z. Physiol. Chem. 355, 279–288.
Hanske, J., Toffey, J., Morenz, A., Bonilla, A., Schiavoni, K., Pletneva, E., 2012. Conformational properties of cardiolipin-bound cytochrome c. Proc. Natl. Acad. Sci. U.S.A. 109, 125–130.
Hess, B., Bekker, H., Berendsen, H., Fraaije, J., 1997. LINCS: a linear constraint solver for molecular simulations. J. Comput. Chem. 18, 1463–1472.
Hess, B., 2002. Determining the shear viscosity of model liquids from molecular dynamics simulations. J. Chem. Phys. 116, 209–217.
Hoch, F., 1992. Cardiolipins and biomembrane function. Biochim. Biophys. Acta 1113, 71–133.
Horvath, S., Daum, G., 2013. Lipids of mitochondria. Prog. Lipid Res. 52, 590–614.

Houtkooper, R.H., Vaz, F.M., 2008. Cardiolipin, the heart of mitochondrial metabolism. Cell. Mol. Life Sci. 65, 2493–2506.
Houtkooper, R.H., Turkenburg, M., Karall, D., Pérez-Cerdá, C., Morrone, A., Malvagia, S., Wanders, R.J., Kulik, W., Vaz, F.M., et al., 2009. The enigmatic role of tafazzin in cardiolipin metabolism. Biochim. Biophys. Acta 1788, 2003–2014.
Humphrey, W., Dalke, A., Schulten, K., 1996. VMD – visual molecular dynamics. J. Mol. Graph. 14, 33–38.
Jarerattanachat, V., Karttunen, M., Wong-ekkabut, J., 2013. Molecular dynamics study of oxidized lipid bilayers in NaCl solution. J. Phys. Chem. B 117, 8490–8501.
Javanainen, M., Martinez-Seara, H., Metzler, R., Vattulainen, I., 2017. Diffusion of integral membrane proteins in protein-rich membranes. J. Phys. Chem. Lett. 8, 4308–4313.
Ji, J., Kline, A.E., Amoscato, A., Samhan-Arias, A.K., Sparvero, L.J., Tyurin, V.A., Tyurina, Y.Y., Fink, B., Manole, M.D., Puccio, A.M., et al., 2012. Lipidomics identifies cardiolipin oxidation as a mitochondrial target for redox therapy of brain injury. Nat. Neurosci. 15, 1407.
Jorgensen, W., Chandrasekhar, J., Madura, J., Impey, R., Klein, M., 1983. Comparison of simple potential functions for simulating liquid water. J. Chem. Phys. 79, 926–935.
Jurkiewicz, P., Olżyńska, A., Cwiklik, L., Conte, E., Jungwirth, P., Megli, F., Hof, M., 2012. Biophysics of lipid bilayers containing oxidatively modified phospholipids: insights from fluorescence and EPR experiments and from MD simulations. Biochim. Biophys. Acta 1818, 2388–2402.
Kagan, V.E., Tyurin, V.A., Jiang, J., Tyurina, Y.Y., Ritov, V.B., Amoscato, A.A., Osipov, A.N., Belikova, N.A., Kapralov, A.A., Kini, V., Vlasova, I.I., Zhao, Q., Zou, M., Di, P., Svistunenko, D.A., 2005. Cytochrome c acts as a cardiolipin oxygenase required for release of proapoptotic factors. Nat. Chem. Biol. 1, 223–232.
Kaminski, G., Friesner, R., Tirado-Rives, J., Jorgensen, W., 2001. Evaluation and reparametrization of the OPLS-AA force field for proteins via comparison with accurate quantum chemical calculations on peptides. J. Phys. Chem. B 105, 6474–6487.
Kates, M., Syz, J.-Y., Gosser, D., Haines, T., 1993. pH-dissociation characteristics of cardiolipin and its 2′-deoxy analogue. Lipids 28, 877–882.
Khandelia, H., Mouritsen, O., 2009. Lipid gymnastics: evidence of complete acyl chain reversal in oxidized phospholipids from molecular simulations. Biophys. J. 96, 2734–2743.
Kulig, W., Olzynska, A., Jurkiewicz, P., Kantola, A.M., Komulainen, S., Manna, M., Pourmousa, M., Vazdar, M., Cwiklik, L., Rog, T., et al., 2015. Cholesterol under oxidative stress ? how lipid membranes sense oxidation as cholesterol is being replaced by oxysterols. Free Radic. Biol. Med. 84, 30–41.
Kulig, W., Cwiklik, L., Jurkiewicz, P., Rog, T., Vattulaine, I., 2016. Cholesterol oxidation products and their biological importance. Chem. Phys. Lipids 199, 144–160.
Kuloglu, M., Ustundag, B., Atmaca, M., Canatan, H., Tezcan, A.E., Cinkilinc, N., 2002. Lipid peroxidation and antioxidant enzyme levels in patients with schizophrenia and bipolar disorder. Cell Biochem. Funct. 20, 171–175.
Lemmin, T., Bovigny, C., Lançon, D., Dal Peraro, M., 2013. Cardiolipin models for molecular simulations of bacterial and mitochondrial membranes. J. Chem. Theory Comput. 9, 670–678.
Lesnefsky, E.J., Minkler, P., Hoppel, C.L., 2009. Enhanced modification of cardiolipin during ischemia in the aged heart. J. Mol. Cell. Cardiol. 46, 1008–1015.
Lidman, M., Pokorná, Š., Dingeldein, A., Sparrman, T., Wallgren, M., Šachl, R., Hof, M., Gröbner, G., 2016. The oxidized phospholipid PazePC promotes permeabilization of mitochondrial membranes by Bax. Biochim. Biophys. Acta 1858, 1288–1297.
Lis, M., Wizert, A., Przybylo, M., Langner, M., Swiatek, J., Jungwirth, P., Cwiklik, L., 2011. The effect of lipid oxidation on the water permeability of phospholipids bilayers. Phys. Chem. Chem. Phys. 13, 17555–17563.
Lucero, H., Robbins, P., 2004. Lipid rafts–protein association and the regulation of protein activity. Arch. Biochem. Biophys. 426, 208–224.
Maciejewski, A., Pasenkiewicz-Gierula, M., Cramariuc, O., Vattulainen, I., Róg, T., 2014. Refined OPLS all-atom force field for saturated phosphatidylcholine bilayers at full hydration. J. Phys. Chem. B 118, 4571–4581.
Maciel, E., Domingues, P., Domingues, M.R.M., 2011. Liquid chromatography/tandem mass spectrometry analysis of long-chain oxidation products of cardiolipin induced by the hydroxyl radical. Rapid Commun. Mass Spectrom. 25, 316–326.
Manna, M., Niemela, M., Tynkkynen, J., Javanainen, M., Kulig, W., Muller, D.J., Rog, T., Vattulainen, I., 2016. Mechanism of allosteric regulation of beta2-adrenergic receptor by cholesterol. eLife 5, e18432.
Mohammadyani, D., Yanamala, N., Arias, A.K.S., Kapralov, A.A., Stepanov, G., Nuar, N., Planas-Iglesias, J., Sanghera, N., Kagan, V.E., Klein-Seetharaman, J., 2018. Structural characterization of cardiolipin-driven activation of cytochrome c into a peroxidase and membrane perturbation. Biochim. Biophys. Acta 1860, 1057–1068.
Mylonas, C., Kouretas, D., 1999. Lipid peroxidation and tissue damage. In Vivo 13, 295–309.
Nosé, S., 1984. A unified formulation of the constant temperature molecular dynamics methods. J. Chem. Phys. 81, 511–519.
Olofsson, G., Sparr, E., 2013. Ionization constants pK_a of cardiolipin. PLoS ONE 8, 1–6.
Pöyry, S., Róg, T., Karttunen, M., Vattulainen, I., 2009. Mitochondrial membranes with mono- and divalent salt: changes induced by salt ions on structure and dynamics. J. Phys. Chem. B 113, 15513–15521.
Paradies, G., Petrosillo, G., Paradies, V., Ruggiero, F., 2009. Role of cardiolipin peroxidation and Ca^{2+} in mitochondrial dysfunction and disease. Cell Calcium 45, 643–650.
Paradies, G., Paradies, V., Benedictis, V.D., Ruggiero, F.M., Petrosillo, G., 2014. Functional role of cardiolipin in mitochondrial bioenergetics. Biochim. Biophys. Acta 1837, 408–417.
Parrinello, M., Rahman, A., 1981. Polymorphic transitions in single crystals: a new molecular dynamics method. J. Appl. Phys. 52, 7182–7190.
Róg, T., Martinez-Siera, H., Munck, N., Orešič, M., Karttunen, M., Vattulainen, I., 2009. Role of cardiolipin in the inner mitochondrial membrane: insight gained through atom-scale simulations. J. Phys. Chem. B 113, 3413–3422.
Róg, T., Orłowski, A., Llorente, A., Skotland, T., Sylvänne, T., Kauhanen, D., Ekroos, K., Sandvig, K., Vattulainen, I., 2016. Data including GROMACS input files for atomistic molecular dynamics simulations of mixed, asymmetric bilayers including molecular topologies, equilibrated structures, and force field for lipids compatible with OPLS-AA parameters. Data Brief 7, 1171–1174.
Runas, K., Malmstadt, N., 2015. Low levels of lipid oxidation radically increase the passive permeability of lipid bilayers. Soft Matter 11, 499–505.
Schlame, M., Rua, D., Greenberg, M., 2000. The biosynthesis and functional role of cardiolipin. Prog. Lipid Res. 39, 257–288.
Schug, Z.T., Gottlieb, E., 2009. Cardiolipin acts as a mitochondrial signalling platform to launch apoptosis. Biochim. Biophys. Acta 1788, 2022–2031.
Schwall, C., Greenwood, V., Alder, N., 2012. The stability and activity of respiratory Complex II is cardiolipin-dependent. Biochim. Biophys. Acta 1817, 1588–1596.
Shinzawa-Itoh, K., Aoyama, H., Muramoto, K., Terada, H., Kurauchi, T., Tadehara, Y., Yamasaki, A., Sugimura, T., Kurono, S., Tsujimoto, K., et al., 2007. Structures and physiological roles of 13 integral lipids of bovine heart cytochrome c oxidase. EMBO J. 26, 1713–1725.
Siani, P., de Souza, R., Dias, L., Itri, R., Khandelia, H., 2016. An overview of molecular dynamics simulations of oxidized lipid systems, with a comparison of ELBA and MARTINI force fields for coarse grained lipid simulations. Biochim. Biophys. Acta 1858, 2498–2511.
Sparagna, G.C., Lesnefsky, E.J., 2009. Cardiolipin remodeling in the heart. J. Cardiovasc. Pharmacol. 53, 290–301.
Tyurina, Y.Y., Poloyac, S.M., Tyurin, V.A., Kapralov, A.A., Jiang, J., Anthonymuthu, T.S., Kapralova, V.I., Vikulina, A.S., Jung, M.-Y., Epperly, M.W., et al., 2014. A mitochondrial pathway for biosynthesis of lipid mediators. Nat. Chem. 6, 542.
van der Paal, J., Neyts, E., Verlackt, C., Bogaerts, A., 2016. Effect of lipid peroxidation on membrane permeability of cancer and normal cells subjected to oxidative stress. Chem. Sci. 7, 489–498.
van Meer, G., Voelker, D., Feigenson, G., 2008. Membrane lipids: where they are and how they behave. Nat. Rev. Mol. Cell Biol. 9, 112–124.
Wong-ekkabut, J., Xu, Z., Triampo, W., Tang, I.-M., Tieleman, D.P., Monticelli, L., 2007. Effect of lipid peroxidation on the properties of lipid bilayers: a molecular dynamics study. Biophys. J. 93, 4225–4236.